APL Photonics

Fabrication and non-destructive characterization of tapered single-ring hollow-core photonic crystal fiber

Cite as: APL Photonics 4, 056105 (2019); https://doi.org/10.1063/1.5093474
Submitted: 21 February 2019 • Accepted: 03 May 2019 • Published Online: 24 May 2019

Riccardo Pennetta, Michael T. Enders, Michael H. Frosz, et al.

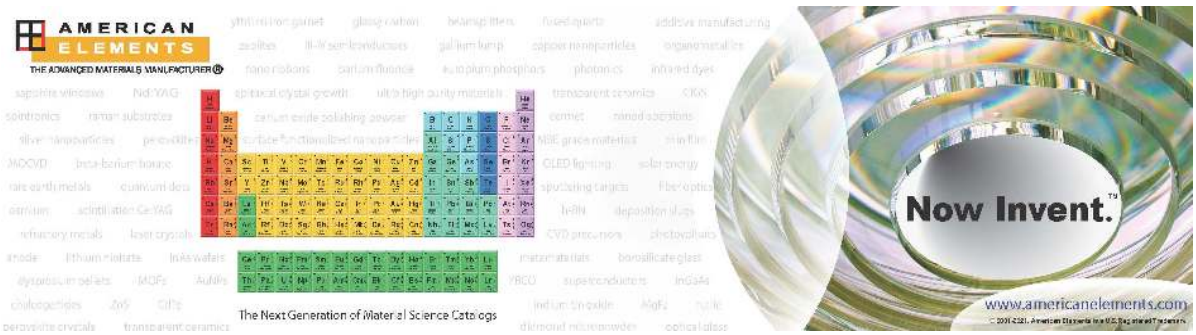

Fabrication and non-destructive characterization of tapered single-ring hollow-core photonic crystal fiber

Cite as: APL Photon. 4, 056105 (2019); doi: 10.1063/1.5093474
Submitted: 21 February 2019 • Accepted: 3 May 2019 •
Published Online: 24 May 2019

Riccardo Pennetta,[a),b)] Michael T. Enders,[a)] Michael H. Frosz, Francesco Tani, and Philip St.J. Russell

AFFILIATIONS

Max Planck Institute for the Science of Light, Staudtstr. 2, 91058 Erlangen, Germany

[a)]**Contributions:** R. Pennetta and M. T. Enders contributed equally to this work.
[b)]**Author to whom correspondence should be addressed:** riccardo.pennetta@mpl.mpg.de

ABSTRACT

We report on the properties of tapered single-ring hollow-core photonic-crystal fibers, with a particular emphasis on applications in nonlinear optics. The simplicity of these structures allows the use of non-invasive side-illumination to assess the quality of the tapering process, by observing the scattered far-field spectrum originating from excitation of whispering-gallery modes in the cladding capillaries. We investigate the conditions that ensure adiabatic propagation in the up- and down-tapers, and the scaling of loss-bands (created by anti-crossings between the core mode and modes in the capillary walls) with taper ratio. We also present an analytical model for the pressure profile along a tapered hollow fiber under differential pumping.

I. INTRODUCTION

Over the last few decades, tapered step-index and photonic crystal fibers, offering axially varying dispersion and high effective nonlinearity, have emerged as attractive platforms for controlling nonlinear optical effects such as supercontinuum generation,[1,2] dispersive wave generation,[3,4] adiabatic pulse compression[5] and third harmonic generation.[6,7] More recently, rapid developments in hollow-core photonic crystal fibers that guide by anti-resonant-reflection (ARR-PCFs) have opened up new possibilities for gas-based nonlinear optics, offering very high optical damage thresholds, wide spectral transmission bands (especially in the UV[8,9] and in the mid-IR[10]) and pressure-tunable dispersion when gas-filled.[11] Here we report on a series of experiments exploring the use of tapered ARR–PCF in gas-based nonlinear optics. Although tapered kagomé ARR-PCFs have previously been reported,[12] their nonlinear properties have so far only been investigated numerically.[13] Among the different types of ARR-PCF,[14] single-ring PCF (SR-PCF), consisting of a circular ring of thin-walled capillaries surrounding a central hollow core and mounted inside a thick-walled fiber capillary, has received great attention recently because it can offer low-loss,[15] easily predictable windows of transparency,[16] effectively single-mode guidance[17] and, not least, is relatively simple to fabricate. We report on the fabrication and characterization of tapered SR-PCF, and present a systematic analysis of the optical properties relevant to experiments in the field of nonlinear optics. We also derive an analytical expression for the pressure profile along the fiber when it is differentially pumped. Finally, we show that the taper profile can be designed so that the zero dispersion wavelength (ZDW) remains constant along the whole fiber length, while the third order dispersion and the effective nonlinearity vary.

II. FABRICATION AND CHARACTERIZATION

A. Tapering technique

A tapered fiber usually consists of a down-taper where the fiber diameter is reduced, followed by a waist of constant diameter and an up-taper to the original diameter. The length of the waist can extend from a few millimeters to several tens of centimeters. We define the local taper ratio T_R as the dimension of a feature in the tapered fiber divided by its value in the untapered fiber. For isomorphic tapering, the aim is to maintain the same value of T_R for all

geometrical features of the microstructure (i.e., core diameter, capillary-wall thickness, etc.).

Tapered fibers are fabricated by scanning an oxy-butane flame along the length of a fiber while gently pulling it. Precise control of the extension of the heated area during the elongation process allows production of arbitrary taper profiles and waist lengths.[18] In the case of SR HC-PCF, since the cladding consists of thin-walled capillaries, heating up the glass often results in collapse of the microstructure, driven by surface tension. To compensate for this, the gas pressure in the hollow regions outside the cladding capillaries was reduced during the taper fabrication, while maintaining the capillaries at atmospheric pressure. This was achieved by collapsing the cladding capillaries at the evacuated fiber end using the electric arc of a fiber splicer while completely sealing the other fiber end with vacuum-compatible epoxy.

To obtain isomorphic tapers, the flame temperature was adjusted (by changing the oxygen concentration in the gas mixture or varying the distance between flame and fiber) to the lowest value that allowed softening of the silica glass. The optimal tapering conditions were found by tapering fresh samples at successively lower values of core pressure until the microstructure scaled isomorphically. A systematic study of different SF-PCFs revealed that the required evacuation pressure (generally in the range 30 mbar–500 mbar) depends non-trivially on the core diameter and the capillary-wall thickness and needs to be carefully calibrated for each SR-PCF geometry. Once the optimal parameters have been found, however, several samples could be successfully tapered even for significantly different values of T_R. During tapering the fiber elongation rate was set to 0.3 mm/s, so that the entire process lasted only a few minutes.

In the following we show experimental results obtained with a five-capillary SR-PCF with a core diameter of 32 μm and a core-wall thickness of ~400 nm. Figure 1 compares scanning electron micrographs (SEM) of the fiber cross-section for (a) $T_R = 1$, (b) $T_R = 0.33$ and (c) $T_R = 0.17$. The microstructure is very well preserved even at high tapering ratios. Direct fiber-drawing of SR-PCF with such small features (below 10 μm core diameter and sub-100 nm capillary wall thickness) is technically very challenging.

B. Characterization of the tapered fiber

Isomorphic scaling of the fiber structure with T_R is in general not guaranteed, and anamorphic deformations are not easily observable by imaging the fiber through the side in an optical microscope. Although cleaving (Fig. 1) allows the local microstructure to be imaged, it destroys the sample. For non-destructive testing, we have exploited a novel technique that allows the local diameter of the cladding capillaries to be measured to sub-micron precision via whispering gallery mode (WGM) resonances.[19] The experimental set-up is shown in Fig. 2(a). The fiber is illuminated from the side using a broadband light source (e.g., a Xe lamp). Part of the light couples to WGMs in the capillaries and is collected by a multimode optical fiber (400 μm core diameter) and delivered to a spectrometer. The capillary diameter D can be calculated by first Fourier transforming the measured optical spectrum to obtain the frequency spacing $\Delta\nu$ between the WGMs, and then applying $D = c/(\pi\Delta\nu n_{WGM})$, where n_{WGM} is related to the effective index of the WGMs.[19] Both the light source and the multimode fiber are mounted on a translation stage, allowing the measurement to be repeated at several positions along the fiber length. The diameter of individual cladding capillaries can be measured by rotating the fiber using two synchronized motorized stages.

As an example, Fig. 2(b) plots T_R for the diameter of one of the cladding capillaries (orange circles, measured via the WGM resonances) and for the outer diameter of the fiber (blue dots, measured using an optical microscope). Both measurements agree very well with the taper design (solid gray line). We point out that a correct scaling of the outer diameter and the diameter of the capillaries is sufficient for isomorphic preservation of the structure.

The transmission spectrum of SR-PCF consists of broad low-loss windows interspersed by narrow high-loss bands caused by anti-crossings between the core mode and leaky open resonances in the capillary walls. The wavelength of the mth order anti-crossing can be predicted to good accuracy by:[16]

$$\lambda_m = \frac{2t}{m}\sqrt{n_g^2 - 1} \tag{1}$$

where t is the capillary wall thickness and n_g is the refractive index of the glass. As predicted by the scalar approximation,[20] isomorphic down-scaling of the microstructure blue-shifts the anti-crossing wavelengths. To verify this, light from a home-built supercontinuum source, based on a solid-core PCF pumped in the anomalous dispersion regime, was launched into several 9-cm-long taper waists (with their transition regions cleaved away) with different values of T_R. Measured transmission spectra for $T_R = 1$, $T_R = 0.76$ and $T_R = 0.45$ [Fig. 3(a)] clearly show the blue-shift of the $m = 1$ anti-crossing wavelength. Figure 3(b) plots the $m = 1$ anti-crossing wavelengths for several different values of T_R, confirming the validity of Eq. (1). The first transmission window shifts to shorter wavelengths, resulting in strong attenuation at longer wavelengths. These features

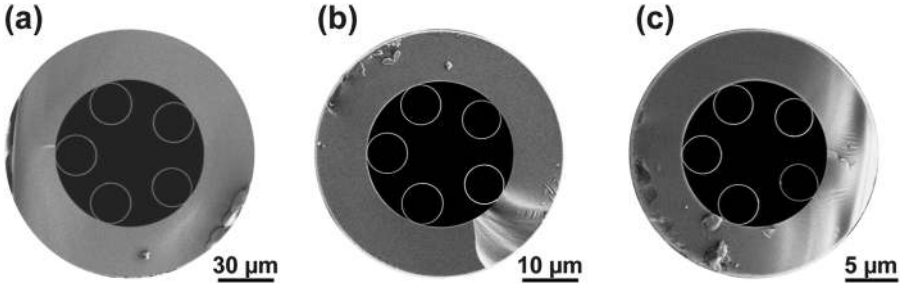

FIG. 1. Scanning electron micrograph (SEM) of the end-face of the SR-PCF for: (a) untapered fibre (core diameter 32 μm, wall thickness 411 nm), (b) fibre with $T_R = 0.33$ (core diameter 11.1 μm, wall thickness 149 nm), (c) fibre with $T_R = 0.17$ (core diameter 5.8 μm, wall thickness 84 nm).

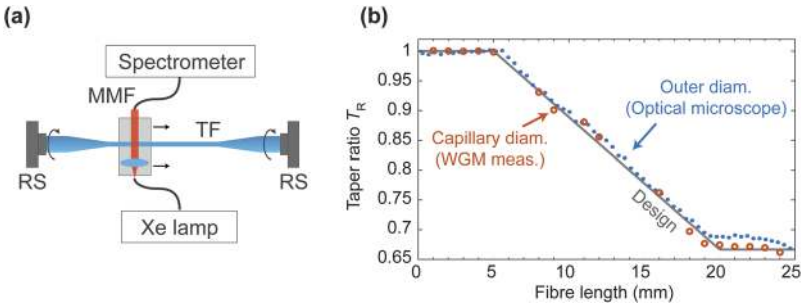

FIG. 2. (a) Experimental setup used to measure the diameter of the cladding capillaries. MMF, multimode fibre; RS, rotational stage; TF, tapered fiber. (b) Taper ratio of the outer diameter (blue dots) and the cladding capillaries diameter (orange circles). The gray line indicates the target taper ratio T_R during the fabrication process. The measurements confirm isomorphic tapering (i.e., all the fiber features scale with the same value of T_R).

suggest that with proper design, tapered gas-filled SR HC-PCFs can be used to control laser frequency conversion,[11] allowing unwanted wavelengths to be suppressed. We observe that the fine structure of the measured spectra around the supercontinuum pump wavelength (1064 nm) depends only on the properties of the light source and is not associated with the waveguide resonances.

To avoid unwanted coupling into higher order and radiation modes, it is important that the up- and down-tapers are adiabatic, i.e., they satisfy the *length-scale criterion*,[21] which limits the maximum allowed taper angle Ω for a given core radius to:

$$\Omega_{\max}(z) = \frac{a(z)}{\lambda}(n_{01} - n_{02}), \tag{2}$$

where z is the axial coordinate, λ is the vacuum wavelength, $a(z)$ is the local core radius, and n_{01} and n_{02} are the local refractive indices of the fundamental (LP_{01}) and first higher-order modes sharing the same azimuthal symmetry (LP_{02}). Away from the anti-crossings, the effective refractive index of the LP_{mn} mode is given to a good approximation by the capillary model:[22]

$$n_{mn}(\lambda,\rho) = \sqrt{n_{gas}^2(\lambda,\rho) - \left(\frac{u_{mn}\lambda}{2\pi a}\right)^2} \approx 1 + \frac{1}{2}\delta(\lambda)\frac{\rho}{\rho_0} - \frac{1}{2}\left(\frac{u_{mn}\lambda}{2\pi a}\right)^2, \tag{3}$$

where ρ is the gas density and ρ_0 its value at standard temperature and pressure (for an ideal gas $\rho/\rho_0 = pT_0/p_0T$, where p is the pressure and T the temperature), δ(λ) is a Sellmeier expansion for the dielectric susceptibility of the gas, and u_{mn} is the nth zero of the mth order Bessel function of the first kind. Combining Eqs. (2) and (3), we obtain:

$$\Omega_{\max}(z) = \frac{\lambda}{8\pi^2 a(z)}(u_{02}^2 - u_{01}^2) = 0.313\frac{\lambda}{a(z)} = 0.313\frac{\lambda}{a_0 T_R(z)}. \tag{4}$$

In Fig. 4(a), $\Omega_{\max}$ is plotted against z/L (solid blue line) at a wavelength of 980 nm for $2a_0 = 32\ \mu$m and a linear taper profile $T_R(z) = (1 - 0.33z/L)$, where L is the taper length. The taper angles corresponding to $L = 5$ mm, 10 mm and 20 mm are, respectively, 2.4, 1.2 and 0.6 mrad, well within the adiabatic region, showing that for this family of tapers adiabatic propagation is ensured. Figure 4(b) shows the measured transmission at 980 nm for four values of L; no degradation in the optical properties is observable.

III. GAS PRESSURE DISTRIBUTION IN TAPERED SR-PCFs

Fiber tapering allows the dispersion and nonlinearity to be tailored along the fiber. Although a similar effect can be obtained by applying different pressures at the two fiber ends,[23] the effect on the fiber properties is different. The chromatic dispersion of the LP_{01}-like guided mode depends on the balance between the anomalous geometrical dispersion of the hollow waveguide and the normal dispersion of the gas, with the result that the $\beta_2 = \partial^2\beta/\partial\omega^2$ becomes less anomalous as the gas pressure is increased. On the other hand, the nonlinear coefficient $\gamma = 2n_2/(\lambda a^2)$ depends linearly on the gas pressure, and inversely on the square of the core radius. Both pressure gradients and tapering can be combined to design systems with a desired distribution of dispersion and nonlinearity.

A pressure gradient can be created by enclosing the two end-faces of the fiber taper in gas cells at different pressures. Most experiments with gas-filled SR-PCFs are performed at pressures above ~10 mbar in the hydrodynamic regime, when intermolecular collisions dominate over collisions with the core wall. In dynamic equilibrium the number of gas molecules flowing per second is constant

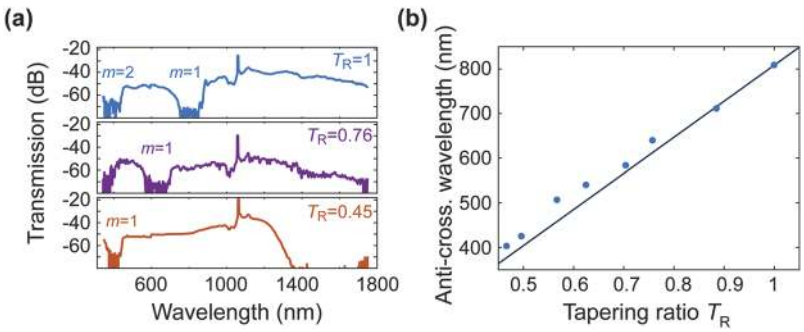

FIG. 3. (a) Transmission spectra through a 9 cm lengths of untapered ($T_R = 1$) and tapered ($T_R = 0.76$ and $T_R = 0.45$) fibers. (b) Measured anti-crossing wavelength of the $m = 1$ anti-crossing as a function of T_R; the dots represent experimental measurements, while the solid line was calculated using Eq. (1).

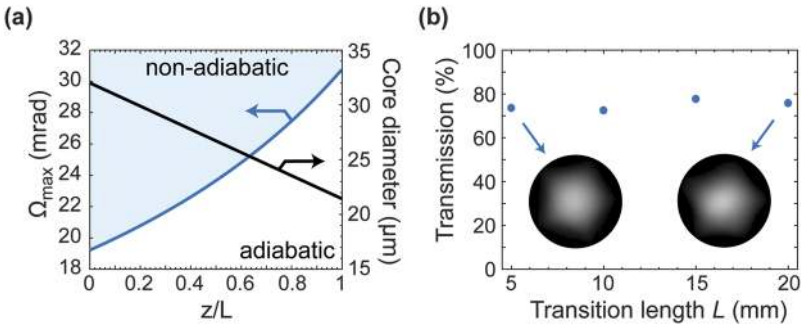

FIG. 4. (a) The maximum tapering angle as a function of normalized position z/L for a taper in which the core diameter varies linearly from 32 to 21.5 μm (blue line). The taper angles corresponding to L = 5 mm, 10 mm and 20 mm are, respectively, 2.4, 1.2 and 0.6 mrad, lying well within the adiabatic region. (b) Measured optical transmission at 980 nm for four different transition lengths L. The insets show the measured near-field mode profiles for L = 5 and 20 mm.

along the taper. Assuming Poiseuille flow (a good approximation in this case[24,25]) and noting that the local gas density (kg/m^2) is proportional to the pressure $p(z)$, the average local flow velocity and mass flow rate can be calculated as:

$$\bar{U}(z) = \frac{a^4(z)\pi}{8\eta}\frac{dp(z)}{dz} \quad \text{and} \quad \dot{m} \propto p(z)\bar{U}(z) \tag{5}$$

assuming isothermal conditions. Solving the second of these equations for constant mass flow, we obtain the pressure distribution:

$$p(z) = \sqrt{p_0^2 - (p_0^2 - p_L^2)\int_0^z a^{-4}(z)dz / \int_0^L a^{-4}(z)dz}, \tag{6}$$

where p_0 and p_L are the pressures at $z = 0$ and L, respectively. For a uniform fiber, Eq. (6) reduces to $p(z) = \sqrt{p_0^2 - z(p_0^2 - p_L^2)/L}$ as expected.[26]

For a general taper profile, Eq. (6) needs to be solved numerically. For illustration we treat the cases of a simple linear down-taper [Fig. 5(a)] and a profile with linear up- and down-tapers and a central waist [Fig. 5(b)]. The calculated pressure distributions for p_0 = 10 bars and p_L = 1 bar are shown by the solid blue curves in the lower panels in Fig. 5. To assess the accuracy of the Poiseuille approximation, we include numerical solutions of the Navier–Stokes equation obtained by finite element modeling (orange curves). In both cases the agreement is good. For comparison we include the solution for an untapered fibre (dashed gray curve). It is evident that a decrease in core diameter offers higher resistance to gas flow and, in the case of Fig. 5(b), decouples the high and low pressure regions.

IV. MANIPULATING THE ZDW

The ZDW plays an important role in the dynamics of nonlinear propagation. As an example of the additional freedom introduced by combining tapering and pressure gradients, we show how to design a fiber taper in which the ZDW stays constant, despite there being a pressure gradient, while at the same time the fibre nonlinearity and dispersion slope vary. In particular, keeping the ZDW constant along the fibre while increasing the nonlinearity can be exploited, for example, for spectral broadening of pulses a few hundred femtosecond in duration by self-phase modulation in the normal dispersion region. Such a configuration would help achieve spectral broadening of a few tens of terahertz within a shorter fibre length, while at the

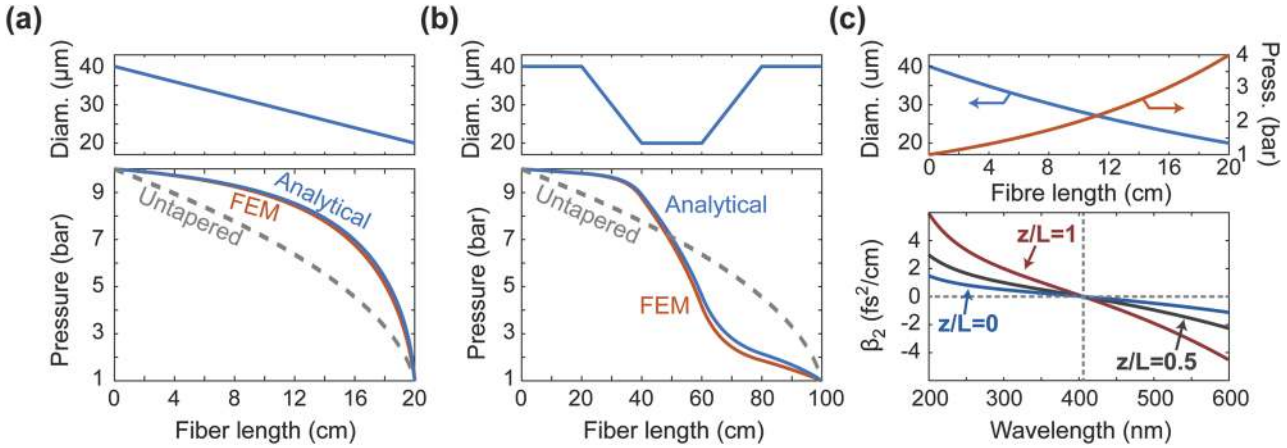

FIG. 5. Gas pressure along the fiber calculated for (a) a linearly decreasing taper transition and (b) a fiber with linear up- and down-tapers and a central waist. The upper panels show the fiber geometries. The grey dashed curves show the pressure distribution in the untapered case. FEM: finite element modeling. (c) Upper panel: taper profile (left axis) and pressure distribution (right axis) for a fiber tapered following Eq. (9). Lower panel: corresponding calculated values of β_2 at z/L = 0 (solid blue line), z/L = 0.5 (solid gray line) and z/L = 1 (solid red line) when argon gas is used to fill the fiber. The vertical dashed gray line indicates the position of the ZDW, while the horizontal dashed gray line marks β_2 = 0.

same time avoiding instabilities such as modulational instability and in-coupling instability, which emerge in the presence of very high nonlinearity at the fibre input.

Using Eq. (3) to calculate β_2 and then setting it to zero yields the condition:

$$a^2(z)p(z) = \frac{u_{mn}p_0}{2\pi^2\partial^2\delta(\lambda)/\partial\lambda^2}. \quad (7)$$

Since none of the quantities on the right-hand side of Eq. (7) depend on T_R or the gas pressure, the taper profile that allows the fiber geometry to be scaled without changing the ZDW can be found by solving Eq. (6) subject to the additional condition:

$$a^2(z)p(z) = a_0^2p_0 = a_L^2p_L \quad (8)$$

which leads to:

$$a(z) = a_L^{z/L}a_0^{1-(z/L)}. \quad (9)$$

We observe in Eq. (9) that the length of the fibre L is an independent parameter and so can be freely chosen, depending on the experimental requirements. As an example, the upper panel in Fig. 5(c) shows the profile and the corresponding pressure distribution for a fiber tapered following Eq. (9). For argon filling-gas, the corresponding calculated values of β_2 at $z/L = 0$, $z/L = 0.5$ and $z/L = 1$ are plotted in the lower panel of Fig. 5(c). It is evident that, while the ZDW remains constant, the third order dispersion varies significantly along the taper.

V. CONCLUSIONS

SR-PCF can be tapered using the standard flame brush technique by selectively evacuating the regions outside the capillaries so as to balance surface tension. SR-PCF structures with small core diameters (<10 μm) and very thin capillary walls (<100 nm), not easily produced by direct fiber drawing, can be routinely fabricated. By shifting loss-inducing anti-crossings into the vacuum ultraviolet, this makes it possible to extend the SR-PCF transparency window deep into the UV. Taper lengths of a few tens of centimeters can be produced—more than enough for many nonlinear optical experiments involving gas-filled SR-PCF.[11] The simple geometry of SR-PCFs allows non-invasive characterization of the microstructure via excitation of WGM resonances in the cladding capillaries. Since suppression of higher order modes, leading to robust single-mode guidance, occurs for $d/(2a) = 0.682$, where d is the inner capillary diameter,[17] this property will persist at every value of T_R. Combining differential pumping with tapering opens up new possibilities for controlling the fiber dispersion and nonlinearity, further improving the flexibility of gas-filled SR-PCFs, especially for applications in nonlinear optics. Other potential applications include optomechanical devices[27,28] and optical trapping,[29] since down-scaling the diameter of the core will strongly increase the optical forces.

REFERENCES

[1] T. A. Birks, W. J. Wadsworth, and P. St. J. Russell, "Supercontinuum generation in tapered fibers," Opt. Lett. **25**, 1415 (2000).

[2] S. P. Stark, J. C. Travers, and P. St. J. Russell, "Extreme supercontinuum generation to the deep UV," Opt. Lett. **37**, 770 (2012).

[3] J. C. Travers and J. R. Taylor, "Soliton trapping of dispersive waves in tapered optical fibers," Opt. Lett. **34**, 115 (2009).

[4] A. V. Gorbach and D. V. Skryabin, "Theory of radiation trapping by the accelerating solitons in optical fibers," Phys. Rev. A **76**, 053803 (2007).

[5] J. C. Travers, J. M. Stone, A. B. Rulkov, B. A. Cumberland, A. K. George, S. V. Popov, J. C. Knight, and J. R. Taylor, "Optical pulse compression in dispersion decreasing photonic crystal fiber," Opt. Express **15**, 013203 (2007).

[6] D. A. Akimov, A. A. Ivanov, A. N. Naumov, O. A. Kolevatova, M. V. Alfimov, T. A. Birks, W. J. Wadsworth, P. St. J. Russell, A. A. Podshivalov, and A. M. Zheltikov, "Generation of a spectrally asymmetric third harmonic with unamplified 30-fs Cr:forsterite laser pulses in a tapered fiber," Appl. Phys. B **76**, 515 (2003).

[7] J. Hammer, A. Cavanna, R. Pennetta, M. V. Chekhova, P. St. J. Russell, and N. Y. Joly, "Dispersion tuning in sub-micron tapers for third-harmonic and photon triplet generation," Opt. Lett. **43**, 2320 (2018).

[8] F. Gebert, M. H. Frosz, T. Weiss, Y. Wan, A. Ermolov, N. Y. Joly, P. O. Schmidt, and P. St. J. Russell, "Damage-free single-mode transmission of deep-UV light in hollow-core PCF," Opt. Express **22**, 015388 (2014).

[9] F. Yu, M. Cann, A. Brunton, W. Wadsworth, and J. Knight, "Single-mode solarization-free hollow-core fiber for ultraviolet pulse delivery," Opt. Express **26**, 010879 (2018).

[10] F. Yu, W. J. Wadsworth, and J. C. Knight, "Low loss silica hollow core fibers for 3-4 micrometre spectral region," Opt. Express **20**, 011153 (2012).

[11] P. St. J. Russell, P. Hölzer, W. Chang, A. Abdolvand, and J. C. Travers, "Hollow-core photonic crystal fibres for gas-based nonlinear optics," Nat. Photonics **8**, 278 (2014).

[12] X. Zheng, B. Debord, L. Vincetti, B. Beaudou, F. Gérôme, and F. Benabid, "Fusion splice between tapered inhibited coupling hypocycloid-core Kagome fiber and SMF," Opt. Express **24**, 014642 (2016).

[13] M. S. Habib, C. Markos, J. E. Antonio-Lopez, R. A. Correa, O. Bang, and M. Bache, "Multi-stage generation of extreme ultraviolet dispersive waves by tapering gas-filled hollow-core anti-resonant fibers," Opt. Express **26**, 024357 (2018).

[14] C. Wei, R. Joseph Weiblen, C. R. Menyuk, and J. Hu, "Negative curvature fibers," Adv. Opt. Photonics **9**, 504 (2017).

[15] B. Debord, A. Amsanpally, M. Chafer, A. Baz, M. Maurel, J. M. Blondy, E. Hugonnot, F. Scol, L. Vincetti, F. Gérôme, and F. Benabid, "Ultralow transmission loss in inhibited-coupling guiding hollow fibers," Optica **4**, 209 (2017).

[16] J. L. Archambault, R. J. Black, S. Lacroix, and J. Bures, "Loss calculations for antiresonant waveguides," J. Lightwave Technol. **11**, 416 (1993).

[17] P. Uebel, M. C. Günendi, M. H. Frosz, G. Ahmed, N. N. Edavalath, J.-M. Ménard, and P. St. J. Russell, "Broadband robustly single-mode hollow-core PCF by resonant filtering of higher-order modes," Opt. Lett. **41**, 1961 (2016).

[18] T. A. Birks and Y. W. Li, "The shape of fiber tapers," J. Lightwave Technol. **10**, 432–438 (1992).

[19] M. H. Frosz, R. Pennetta, M. T. Enders, G. Ahmed, and P. St. J. Russell, "Non-invasive real-time characterization of hollow-core photonic crystal fibres using whispering gallery mode spectroscopy," in CJ-3.6, CLEO Europe, Munich, Germany, 2019.

[20] T. A. Birks, D. M. Bird, T. D. Hedley, J. M. Pottage, and P. St. J. Russell, "Scaling laws and vector effects in bandgap-guiding fibres," Opt. Express **12**, 69 (2004).

[21] J. D. Love, W. M. Henry, W. J. Stewart, R. J. Black, S. Lacroix, and F. Gonthier, "Tapered single-mode fibers and devices: 1. Adiabaticity criteria," IEE Proc.-J: Optoelectron. **138**, 343 (1991).

[22] M. A. Finger, N. Y. Joly, T. Weiss, and P. St. J. Russell, "Accuracy of the capillary approximation for gas-filled kagomé-style photonic crystal fibers," Opt. Lett. **39**, 821 (2014).

[23] K. F. Mak, J. C. Travers, P. Hölzer, N. Y. Joly, and P. St. J. Russell, "Tunable vacuum-UV to visible ultrafast pulse source based on gas-filled kagome-PCF," Opt. Express **21**, 010942 (2013).

[24] *Handbook of Vacuum Technology*, edited by K. Jousten (Wiley-VCH Verlag GmbH & Co. KGaA, 2016).

[25] L. B. Loeb, *The Kinetic Theory of Gases* (Courier Corporation, 2004).

[26] A. Suda, M. Hatayama, K. Nagasaka, and K. Midorikawa, "Generation of sub-10-fs, 5-mJ-optical pulses using a hollow fiber with a pressure gradient," Appl. Phys. Lett. **86**, 111116 (2005).

[27]S. Xie, R. Pennetta, and P. St. J. Russell, "Self-alignment of glass fiber nanospike by optomechanical back-action in hollow-core photonic crystal fiber," Optica **3**, 277–282 (2016).
[28]R. Pennetta, S. Xie, F. Lenahan, M. Mridha, D. Novoa, and P. St. J. Russell, "Fresnel-reflection-free self-aligning nanospike interface between a step-index fiber and a hollow-core photonic-crystal-fiber gas cell," Phys. Rev. Appl. **8**, 014014 (2017).
[29]R. Zeltner, R. Pennetta, S. Xie, and P. St. J. Russell, "Flying particle micro-laser and temperature sensor in hollow-core photonic crystal fiber," Opt. Lett. **43**, 1479–1482 (2018).